CHEMISTRY
A EUROPEAN JOURNAL

DOI: 10.1002/chem.200501389

Optical, Redox, and NLO Properties of Tricyanovinyl Oligothiophenes: Comparisons between Symmetric and Asymmetric Substitution Patterns

Juan Casado,[a] M. Carmen Ruiz Delgado,[a] M. Carmen Rey Merchán,[a] Víctor Hernández,[a] Juan T. López Navarrete,*[a] Ted M. Pappenfus,[b] Nathaniel Williams,[b] William J. Stegner,[b] Jared C. Johnson,[b] Brett A. Edlund,[b] Daron E. Janzen,[c] Kent R. Mann,[c] Jesús Orduna,[d] and Belén Villacampa[e]

Abstract: A series of tricyanovinyl (TCV)-substituted oligothiophenes was synthesized and investigated with a number of physical methods including UV/Vis, IR, and Raman spectroscopy, nonlinear optical (NLO) measurements, X-ray diffraction, and cyclic voltammetry. Mono- or disubstituted oligomers were prepared by the reaction of tetracyanoethylene with mono- or dilithiated oligomers. The comparative effects of the symmetric and asymmetric substitutions in the electronic and molecular properties have been addressed. These oligomers display dramatic reductions in both their optical and electrochemical band gaps in comparison with unsubstituted molecules. The analysis of the electronic properties of the molecules was assisted by density functional theory calculations, which are in excellent agreement with the experimental data. TCV substitution influences the energies of the frontier orbitals, especially with respect to the stabilization of LUMO orbitals. X-ray structural characterization of a monosubstituted oligomer exhibits π-stacking with favorable intermolecular interactions. NLO results agree with the role of the intramolecular charge-transfer feature in the asymmetric samples. These results furthermore exalt the role of conformational flexibility in the disubstituted compounds and reveal an unexpected nonlinear optical activity for symmetric molecules. Regarding the electronic structure, the interpretation of the vibrational data reflects the balanced interplay between aromatic and quinoid forms, finely tuned by the chain length and substitution pattern. The electronic and structural properties are consistent with the semiconducting properties exhibited by these materials in thin film transistors (TFTs).

Keywords: electronic structure · oligothiophenes · photonics · semiconductors

[a] Dr. J. Casado, M. C. Ruiz Delgado, M. C. Rey Merchán, Prof. V. Hernández, Prof. J. T. López Navarrete
Department of Physical Chemistry, University of Málaga
Campus de Teatinos s/n, Málaga 29071 (Spain)
Fax: (+34) 952-13-000
E-mail: teodomiro@uma.es

[b] Dr. T. M. Pappenfus, N. Williams, W. J. Stegner, J. C. Johnson, B. A. Edlund
Division of Science and Mathematics
University of Minnesota, Morris, MN 56267 (USA)

[c] Dr. D. E. Janzen, Prof. K. R. Mann
Department of Chemistry, University of Minnesota
Minneapolis, MN 55455 (USA)

[d] Prof. J. Orduna
Department of Organic Chemistry, ICMA
University of Zaragoza-CSIC, Zaragoza 50009 (Spain)

[e] Prof. B. Villacampa
Department of Condensed Mater Physics, ICMA
University of Zaragoza-CSIC, Zaragoza 50009 (Spain)

Introduction

Linear π-conjugated oligomers (e.g., oligothiophenes) are the focus of intense research because they exhibit a variety of interesting optical, electrical, and photoelectrical properties.[1,2] These molecules have been applied as organic semiconductors in electronics,[3] emitters and photovoltaic cells in photonics,[4] and their rich nonlinear optical responses have been used for the construction of electrooptical devices.[5] In general, one of the most advantageous features of organic functional materials is the ease of processing and the tunability of their intrinsic properties through "simple" chemical modifications. The rational design of the chemical architectures of linearly conjugated oligothiophenes concerns itself principally with the functionalization of the two α-terminal positions and with the π-conjugation chain length (i.e., the number of conjugated thiophene rings). The

substitution of the β sites of the thiophene building blocks improves their processability (namely, inclusion of solubilizing groups), a matter of special importance in the case of large oligomers.

Some oligothiophenes have been designed to exhibit intramolecular charge transfer (ICT),[6] achieved by means of α,α′-substitution with electron-donating (D) or electron-accepting (A) moieties, namely, push–pull D-π-A oligothiophenes. Much less attention has been devoted to their symmetric homologues, A-π-A molecules,[7] although they can show noticeable two-photon absorption properties. Molecules with a large two-photon absorption cross section are in great demand for a variety of applications (two-photon excited fluorescence microscopy,[8] optical limiting,[9] three-dimensional optical data storage,[10] etc.). Interestingly, if these optical properties could be combined with other relevant electrical features (such as ambipolar conductivities, as displayed in a symmetric dicyanomethylene-substituted quinoidal oligothiophene),[11] new materials could emerge with additional technological potential.

It is our main purpose in this work to provide an understanding of the molecular and electronic properties of two groups of linearly conjugated oligothiophenes with different chain lengths (trimers (3T) and hexamers (6T)) with either D-π-A or A-π-A substitution patterns. Each group consists of the following: 1) an unsubstituted oligothiophene in which the oligothienyl core acts both as the mediating π-system and as donor (D); 2) a monosubstituted tricyanovinyl (TCV) oligomer, in which TCV is the acceptor (A) to create a D-π-A system; and 3) a disubstituted TCV oligomer of the form A-π-A. A variety of physical methods were used to better understand the properties of these molecules, including spectroscopic (UV/Vis electronic absorption, and vibrational IR and Raman), electrochemical (cyclic voltammetry), and solid state (single-crystal X-ray diffraction) techniques. In addition, this information has been augmented with that provided by the nonlinear optical experiments, and supported or analyzed by using theoretical data (i.e., quantum-chemical density functional theory calculations).

It has been demonstrated that the use of tricyanovinyl acceptors in ICT-conjugated molecules induces a dramatic enhancement of the first-order hyperpolarizability.[12] However, the implementation of tricyanovinyl substitution within oligothiophenes has only recently been addressed.[13] These studies have focused on the synthesis, physical studies and semiconducting properties of the disubstituted TCV-oligothiophenes. For example, the implementation of TCV-3T-TCV in organic field-effect transistor (OFET) devices leads to a reasonably good electron mobility and an on/off ratio of 0.023 $cm^2 V^{-1} s^{-1}$ and 10^6, respectively. On the other hand, TCV-6T-TCV unexpectedly displays an inversion of the majority of charge carriers with a hole mobility of 1×10^{-4} $cm^2 V^{-1} s^{-1}$.[13c] This seemingly puzzling behavior prompted us to perform the present work with the main scope of obtaining a better understanding of the molecular structure/property relationships in these new materials regarding their electronic and optical properties. The interest and significance of the work rely on the accurate analysis of the molecular level features, and is based on a multidisciplinary approach consisting of spectroscopic techniques, electrochemistry, solid-state characterization, and quantum chemistry. In addition, NLO properties of these materials were studied in terms of comparisons between A←D→A and D→A charge-transfer patterns. To our knowledge, such an investigation has yet to be reported. Analyses of this type are important in the design and understanding of new materials for organic-based devices covering a broad range of electrooptical applications.

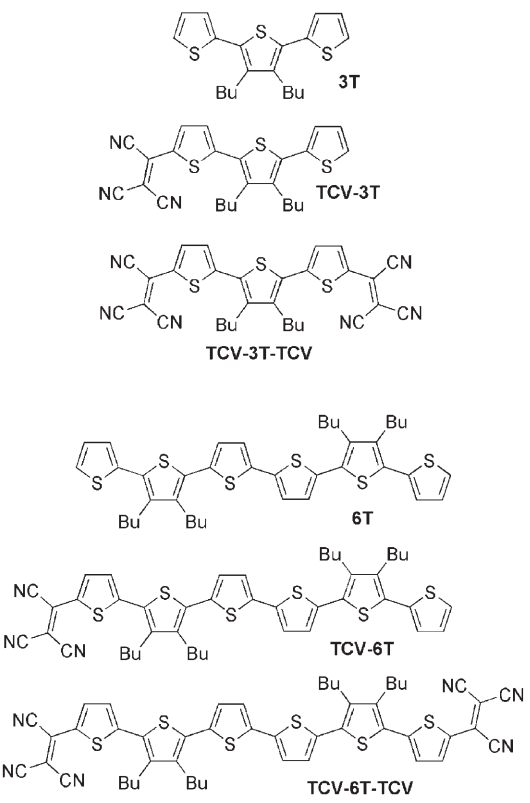

Results and Discussion

Synthesis of oligomers: The synthesis of the unsubstituted and disubstituted oligomers TCV-3T-TCV and TCV-6T-TCV has been reported previously.[13a] A similar approach was utilized for the synthesis of monosubstituted oligomers and is outlined in Scheme 1. Dibutylterthiophene (3T) or tetrabutylsexithiophene (6T) were each treated with one equivalent

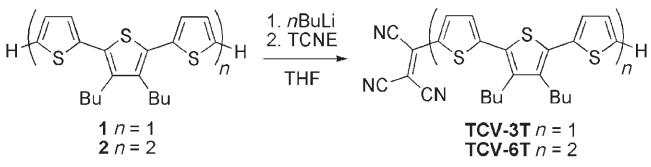

Scheme 1. Synthesis of TCV-3T and TCV-6T

of *n*-butyllithium at low temperature in an attempt to obtain monolithiated species. The resulting anions were treated with tetracyanoethylene to afford TCV-3T and TCV-6T in low to moderate yields. Low yields are attributed to the formation of dilithiated species, as evidenced by the presence of disubstituted oligomers in thin-layer-chromatography experiments. However, the amounts of disubstituted oligomers formed in these reactions were not quantified.

Electronic spectra and orbital topologies: Figure 1 displays the normalized absorption spectra of the substituted compounds, with the values summarized in Table 1. The spectrum of TCV-3T shows an intense band with a maximum at 571 nm (2.17 eV), which is associated with a one-electron HOMO→LUMO transition calculated at 2.29 eV (oscillator strength, $f=0.85$) at the DFT/B3LYP/6–31G** level of theory. The frontier orbitals of TCV-3T (Figure 2) indicate that its HOMO is mainly located over the terthienyl core, while the LUMO is concentrated mostly within the TCV moiety. As a result, this HOMO→LUMO excitation has a large 3T→TCV charge-transfer character, in which the thiophene unit linked to the acceptor acts as the overlapping path of the transition, and accounts for the large intensity. For the disubstituted compound, the lowest energy band, also corresponding to a HOMO→LUMO one-electron excitation, is measured at 583 nm (2.13 eV) and calculated at the same energy (2.13 eV).

A second weaker and broad band centered at 318 nm (3.90 eV) in TCV-3T can emerge from the overlapping of the HOMO−2→LUMO and HOMO→LUMO+1 excitations calculated at 3.21 eV ($f=0.15$) and at 3.62 eV ($f=0.07$), respectively. The second lowest energy band in TCV-3T-TCV at 320 nm (3.88 eV) is calculated at 3.37 eV with a different origin than that of the monosubstituted case, namely HOMO−1→LUMO+1 excitation. This effect will be explained later when the MO level crossing in Figures 2 and 3 is accounted for.

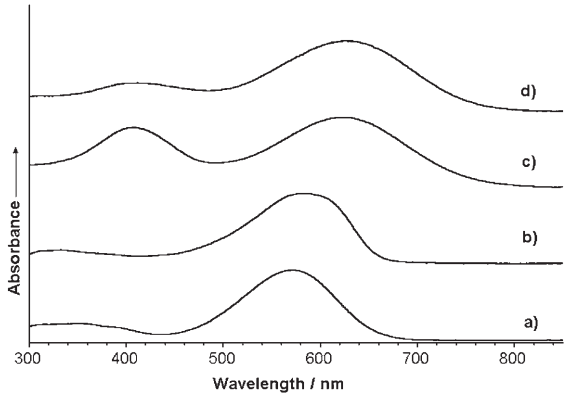

Figure 1. Absorption spectra in CH_2Cl_2 of a) TCV-3T, b) TCV-3T-TCV, c) TCV-6T, d) TCV-6T-TCV.

Table 1. Physical properties of tricyanovinyl oligothiophenes.[a]

	Electronic Data[b]	Electrochemical Data[c]	
	λ_{max} [nm (eV)]	Oxidation $E°$ [V]	Reduction $E°$ [V]
3T[d]	336 (3.69)	1.11[e]	[f]
6T[d]	411 (3.02)	0.81, 0.97, 1.94[e,g]	[f]
TCV-3T	571 (2.17)	1.39[e]	−0.45, −1.13
TCV-6T	624 (1.99)	0.90, 1.12	−0.44, −1.11
TCV-3T-TCV[d]	583 (2.13)	1.72[e]	−0.36[g], −1.33[g,h]
TCV-6T-TCV[d]	628 (1.97)	1.04, 1.27	−0.45[g], −1.13[g]

[a] Butyl-substituted oligomers. [b] Measured in anhydrous dichloromethane. [c] Potentials vs. Ag/AgCl in 0.1 M $TBAPF_6/CH_2Cl_2$ solution. [d] Values from reference 13a. [e] Irreversible process; E_{pa} value provided. [f] No observable reduction processes under the experimental conditions. [g] Number of transferred electrons $n=2$. [h] Irreversible process; E_{pc} value provided.

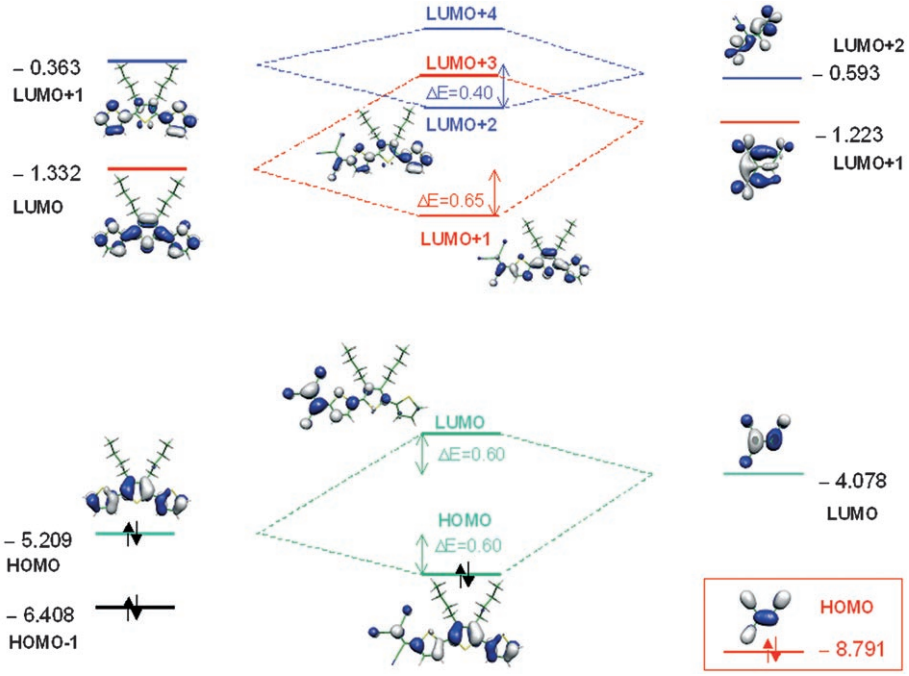

Figure 2. B3LYP/6–31G** molecular orbital diagram of the coupling between TCV-H and 3T fragments. The HOMO data of TCV-H in red indicate no mixing with the frontier orbital of 3T. Double-headed arrows indicate the extension of the coupling.

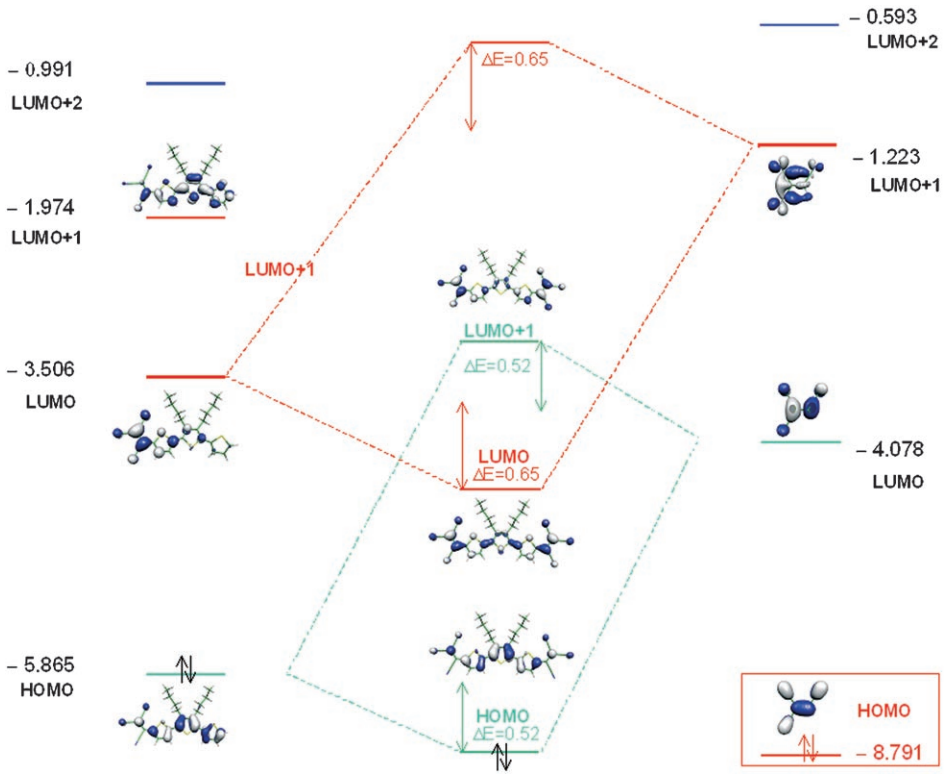

Figure 3. B3LYP/6–31G** molecular orbital diagram of the coupling between TCV-H and TCV-3T fragments.

Figure 2 displays the MO diagram describing the interaction between TCV-H (tricyanoethane) and the terthiophene unit. Both the HOMO and LUMO energies are stabilized in TCV-3T in comparison with those of 3T (much more dramatically in the case of the LUMO). The attachment of a second TCV group results in a further stabilization (≈0.6 eV) for both frontier orbitals of TCV-3T (Figure 3). Let us now quantitatively account for the main reasons for this behavior. To this end, it is necessary to consider the energies and topologies of the doubly occupied HOMO and the empty LUMO frontier orbitals of the two coupling moieties (Figure 2). Given a pair of interacting groups, the extent of the interaction of their orbitals depends on two main factors: 1) the values of the linear combination of atomic orbital (LCAO) coefficients and the symmetry of the MO term (which defines the bonding or antibonding character) of the connecting C atoms, and 2) the relative energy position (energy difference) of the two interacting levels.

Considering the HOMO of TCV-H, the largest interaction is expected to take place with the doubly occupied π molecular orbitals of 3T of similar energies (i.e., near −8.8 eV); hence, the interaction of the TCV-H HOMO with the HOMO of 3T is expected to be negligible. The opposite is expected to occur for the interaction between the LUMO of TCV-H and the HOMO of 3T, since they are much closer in energy. The coupling between the HOMO of 3T and the LUMO of TCV-H thus results in:

1) A doubly occupied level (HOMO of TCV-3T) due to their bonding interaction, with a moderate stabilization by 0.6 eV relative to the HOMO of 3T.
2) An empty molecular orbital due to their antibonding combination, with an energy level above the LUMO of TCV-H offset by 0.6 eV. The latter orbital becomes the LUMO of the coupled system, thus justifying its strong stabilization with respect to the LUMO of 3T.
3) The relative energies also determine that the LUMO of 3T couples with the LUMO+1 of TCV-H, leading to an unoccupied LUMO+1 orbital of TCV-3T, the topology and energy of which resemble those of the LUMO of 3T.
4) This orbital connection allows us to relate the HOMO→LUMO+1 band at 3.90 eV in TCV-3T with the HOMO→LUMO band in nonsubstituted 3T, found at 3.70 eV.[6b,12,13]

Furthermore, this description shows the effect of substitution of a conjugated backbone with a strong acceptor group in terms of inclusion of a new energy level in the former HOMO–LUMO energy gap of the unsubstituted system (i.e., this description could be named *molecular doping* when seen in the light of the similarity with the doping process in inorganic semiconductors). The next LUMO+2 orbital, however, is not the term corresponding to the antibonding LUMO(3T)/LUMO+1(TCV-H) combination, but the result of the bonding coupling between the next two orbitals, LUMO+1(3T)/LUMO+2(TCV-H). At higher energies, the orbital mixing is increasingly extensive.

This theoretical description reveals that no significant role is played by the 3T LUMO in the LUMO of TCV-3T. Furthermore, it highlights two interesting points: 1) the HOMO of TCV-3T is mainly accounted for by the terthienyl core (3T HOMO energy of −5.209 eV and TCV-3T HOMO energy of −5.865 eV); and 2) the LUMO of TCV-3T is mainly accounted for by the tricyanovinyl unit (TCV-H LUMO energy of −4.078 eV and TCV-3T LUMO energy of −3.506 eV). Furthermore, as a result of the interaction between the HOMO of 3T and the LUMO of TCV-H, a certain 3T→TCV electron-density polarization can be anticipated to occur. This is a consequence of the partial occupation of the empty orbital of the acceptor at the expense of

the fully occupied HOMO of 3T. This fact outlines the donor–acceptor interaction that accounts for the ground-state electronic structure of this molecule and will have important consequences on the electrochemical and vibrational properties (vide infra). Another interesting distinction is that the HOMO→LUMO photoelectron excitation really corresponds to a virtual displacement of the electron density from one side of the molecule to the other, that is, a charge-transfer (CT) exciton with seemingly effective electron–hole separation. The HOMO−1→LUMO+1 corresponds, however, to a chain-centered Frenkel exciton in analogy to the HOMO→LUMO exciton character observed in nonsubstituted oligothiophenes.

If one now takes the TCV/TCV-3T pair in Figure 3 into account, the same type of coupling as previously described (HOMO of TCV-3T, −5.865 eV and LUMO of TCV-H, −4.078 eV) must be considered in order to construct a consistent MO energy sequence. It should be noted that the HOMO electron density of the disubstituted system results from a partial filling of the empty TCV-H by part of the occupied HOMO of the monosubstituted molecule. As a result, the HOMO orbital topology of TCV-3T-TCV closely resembles that of TCV-3T, but with the electron density concentrated on the terthiophene core (Figure 4) due to the competition of two electron-withdrawing groups towards the 3T core. This partially prevents a sizeable 3T↔TCV interaction in TCV-3T-TCV, as compared with that noticed in TCV-3T. The LUMO of TCV-3T-TCV (Figure 4) now originates from the LUMO of TCV-3T (rather than from the HOMO of 3T in the case of TCV-3T). Consequently, it turns out that: 1) the HOMO–LUMO energy difference in the disubstituted molecule is only slightly changed with respect to the HOMO–LUMO gap in TCV-3T; and 2) the LUMO of TCV-3T-TCV is quite different from that of TCV-3T, as noticed from the further spreading of the LUMO of TCV-3T-TCV over the entire molecule.

Additionally, this analysis of the MO energy diagram shows an increasing crossing of MO levels (note that for TCV-3T-TCV the LUMO orbital does not meet its origin in the antibonding combination of the TCV-3T HOMO and TCV-H LUMO, but from the bonding interaction between the respective upper LUMO and LUMO+1). This effect also leads to a diminishing energy difference between successive empty levels, which will have important implications in the electrochemical properties. The above predictions are nicely confirmed by the experimental data, which accounts for the

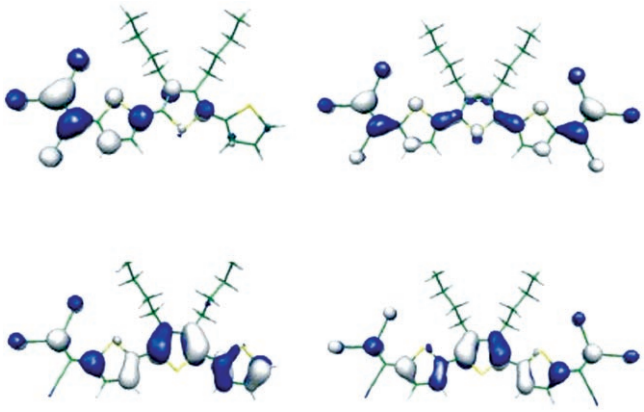

Figure 4. Orbital topologies calculated at the B3LYP/6–31G** level of calculation for the HOMOs (below) and the LUMOs (above) of TCV-3T (left) and TCV-3T-TCV (right).

large red shift in the wavelength of the HOMO–LUMO band from 336 nm in 3T to 571 nm in TCV-3T and the much more moderate shift to 583 nm in TCV-3T-TCV.

In the hexamer homologues, a similar diagram of bonding/antibonding levels is relevant, but with an additional consideration (Figure 5). The increase of the conjugation path from three thiophene units to six leads to a destabilization of the HOMO by ≈0.7 eV. This fact implies that the two interacting terms (i.e., HOMO of 6T and LUMO of TCV-H) are now much closer in energy than in the case of the analogous trimer. The final HOMO–LUMO energy gap is therefore significantly lowered as a consequence of the highly extended π-conjugated path. A similar trend is theoretically expected for the optical bands for both parent trimers and hexamers upon successive grafting of TCV moieties, though displaced towards lower energies in the case of the longer molecules.

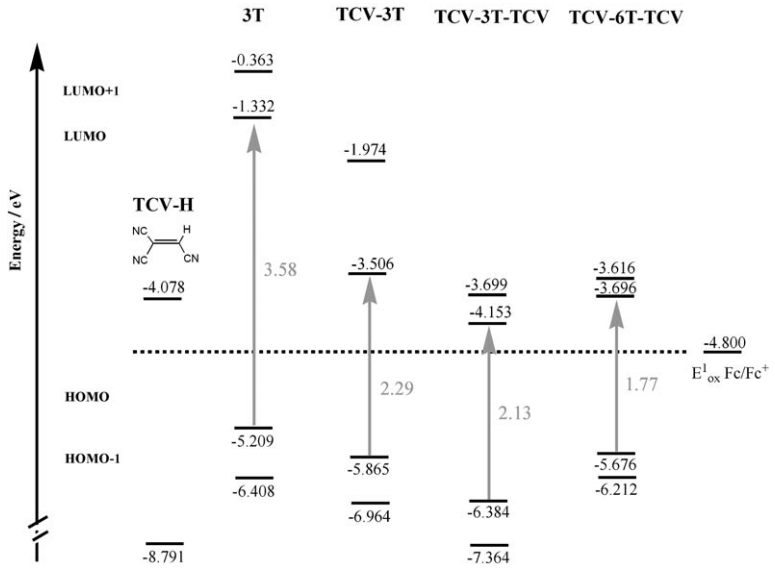

Figure 5. B3LYP/6–31G** absolute energy values for the molecular orbitals around the energy gap. Arrows denote the HOMO→LUMO transition with oscillator strengths.

These DFT/B3LYP/6–31G** predictions complement experimental data similar to the wavelength progressions of the HOMO–LUMO bands for the 6T→TCV-6T→TCV-6T-TCV (411→624→628 nm) and 3T (336→571→583 nm) series. Another consequence of the increment of electron correlation (π conjugation) in longer oligothiophenes is the mixing of configurations describing the photon excitations. This mixing may be at the origin of the distinct nature of the main components that describe the two absorptions near 320 nm in TCV-3T/TCV-3T-TCV and 407 nm in TCV-6T/TCV-6T-TCV.

Electrochemical analysis: Figure 6 shows the redox properties of the TCV-substituted oligomers (see Table 1 for potential values). The data for the disubstituted oligomers

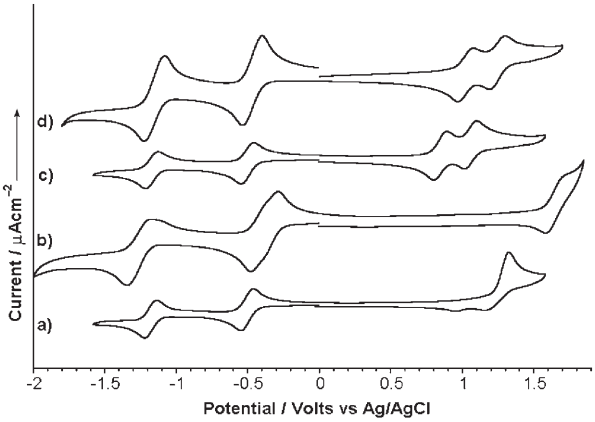

Figure 6. Cyclic voltammograms of a) TCV-3T, b) TCV-3T-TCV, c) TCV-6T, d) TCV-6T-TCV in 0.1 M $TBAPF_6/CH_2Cl_2$, $\nu = 100\,mV\,s^{-1}$. Data for disubstituted molecules are taken from reference [13a].

were reported previously.[13a] Addition of one TCV group to the α-position of the 3T chain results in the appearance of two reversible one-electron reductions, and pushes the irreversible electrochemical oxidation of 3T (1.11 V)[14] to higher potential (1.39 V). These phenomena reflect the dual behavior of the TCV group regarding both the reduction (acting as an acceptor) and the oxidation (acting as an electron-withdrawing unit) processes.

Koopmans' approach[15] enabled us to relate the absolute HOMO–LUMO energies with the electrochemical oxidation–reduction potentials (see Figures 2–4). In this way, reduction reactions can be visualized as the addition of electrons in the empty LUMO, whereas oxidation reactions remove electrons from the fully occupied HOMO. The feature of the LUMO of TCV-3T, which is mainly described by the original empty LUMO of TCV-H, explains the appearance of reductions upon substitution of the cathodically inactive 3T. On the other hand, the 3T→TCV charge polarization in the HOMO removes electron density from the oligothienyl chain and electron extraction becomes more energetic, that is, the electron-withdrawing nature of the TCV plays a role in the anodic processes due to the stabilized HOMO energy levels.

Oxidation of TCV-3T is likely to be followed by a dimerization reaction through coupling at the free α-carbon position. This process was confirmed by the coincidence of the potential values of the two reverse peaks associated with the irreversible oxidation of TCV-3T, and the two reverse peaks related with the two one-electron reversible oxidations of the dimerized molecule TCV-6T-TCV. These two reversible oxidations in the disubstituted hexamer are at higher potentials with respect to TCV-6T, due to the presence of two electron-withdrawing centers. In TCV-6T, the two anodic processes are also reversible, thus accounting for the high stability of the generated radical cation, and the fact that no dimerization is observed on the CV timescale.

The reduction features in the disubstituted systems are both net two-electron processes (direct formation of dianions), contrary to the two one-electron reductions in the case of the monosubstituted compounds. This is theoretically supported in Figures 3 and 4 by the occurrence of two almost degenerate empty levels (LUMO and LUMO+1) in TCV-6T-TCV, while these two levels are ≈0.5 eV apart in TCV-3T-TCV. This separation accounts for the observation of two shoulders in the first electron reduction of TCV-3T-TCV. The one-step dianion formation can be viewed qualitatively as due to the predominance of the TCV-acceptor character of these two orbitals in the disubstituted systems, while the number of thiophene units plays a secondary role. Evidently, the potentials required for the total generation of the successive dianions show a dependence on the chain length. The origin of this dependence is not an intrinsic molecular feature, but a consequence of the more effective mitigation of electrostatic repulsions in a larger system.

Koopmans' theorem can also be applied toward some additional comparisons: 1) Oxidations are shifted to higher potentials upon TCV substitution and reflects the stabilization of HOMO energy levels. 2) TCV-3T-TCV is the easiest molecule within the series to reduce and is in agreement with the theoretical results (vide supra). 3) Lengthening of the chains in the disubstituted samples stabilizes/destabilizes oxidation/reduction in agreement with the predicted destabilizations of both frontier orbitals of TCV-3T-TCV and TCV-6T-TCV.

X-ray crystallographic analysis: Single crystals of TCV-3T were obtained and the solid-state structure solved. Structural data have already been reported for TCV-3T-TCV, and will be used here for comparisons.[13a] Although each molecule in TCV-3T-TCV adopts a *transoid* orientation of the sulfur atoms of adjacent thiophene rings, a *cisoid*/*transoid* (58:42 ratio) disorder exists which affects the outermost ring of TCV-3T. Gas-phase B3LYP/6–31G** calculations reveal a very small energy difference between the two conformations observed in TCV-3T, which agrees with: 1) the occurrence of an almost 50:50 distribution of conformers, and 2) the conformational flexibility as deduced from the nonlinear

optical experiments in the presence of an intense electromagnetic field (vide infra).

Molecules in both systems are nearly flat, with mean deviations from planarity (least-square analysis) of 0.153 and 0.115 Å in TCV-3T-TCV, and even more planar in the monosubstituted molecule, with deviations of 0.068 and 0.065 Å. Both systems π-stack with similar average stacking of 3.57 and 3.55 Å for TCV-3T and TCV-3T-TCV, respectively (see Figure 7). The TCV-3T molecules pack in such a way that

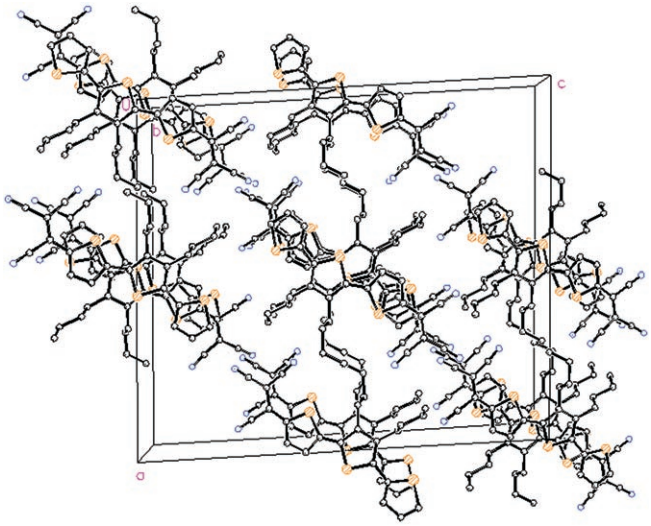

Figure 7. Packing of TCV-3T viewed down the π-stacking axis (transoid conformation is shown exclusively for clarity).

nearest neighbor molecules in the stack have the center thiophene ring pointing in opposite directions. The tricyanovinyl groups associate in regions between the π stacks. As for intramolecular parameters, theory (i.e., gas phase) reproduces the experimental values (i.e., solid state) of TCV-3T quite well (see Figure 13 below): 1) Conjugated C−C/C=C thienyl bond lengths are calculated with an averaged deviation of 0.010 Å. Theory/experiment differences for the TCV fragment are more pronounced, probably due to the interplay of intermolecular interactions promoted by the CN groups in the solid phase. 2) On the other hand, solid-state packing must force molecules to be more planar than calculations actually predict. Theory correctly evaluates, however, the dihedral angle trends. For example, the angle closest to the TCV is calculated to be 10.0°, while that observed experimentally is 12.1°. Meanwhile, the distortion affecting the outer dihedral of the unsubstituted ring is overestimated by calculations (40° by DFT//B3LYP/6–31G** versus 16.0° for the experimental value).

Nonlinear optical properties: The nonlinear optical response of tricyanovinyl thiophenes, determined by electric-field-induced second-harmonic generation (EFISHG), is gathered in Table 2, along with the results of theoretical calculations performed on these molecules. A comparison of the experimental and theoretical hyperpolarizabilities of TCV-3T and TCV-6T reveals that reasonable agreement exists. It must be noted that the $\mu\beta(0)$ values have been calculated on the lowest energy conformations and are therefore larger than those measured in solution where some conformational disorder is expected.

Table 2. Nonlinear optical properties of tricyanovinyl oligothiophenes.

	Experimental[a]		Theoretical			
	$\mu\beta$[b]	$\mu\beta(0)$[b,c]	E_{12} [eV][d]	μ_{12} [D][d]	$\Delta\mu_{12}$ [D][d]	$\mu\beta(0)$[b,e]
TCV-3T	1460	852	2.29	9.9	19.1	1534
TCV-6T	5070	2586	1.64	9.9	55.0	3676
TCV-3T-TCV	650	369	2.13	13.4	0.54	2
syn-TCV-3T-TCV			2.21	10.05	5.90	1004
			2.51	3.18	5.50	
TCV-6T-TCV	2900	1464	1.77	15.35	0	0
syn-TCV-6T-TCV			1.73	9.07	23.01	4251
			1.84	5.52	24.28	

[a] In CH_2Cl_2. [b] 10^{-48} esu. [c] Calculated using a two level model. [d] TD-B3LYP/6–31G**. [e] HF/6–31G**.

Furthermore, we have found that the calculation of coupled perturbed Hartree–Fock (CPHF) hyperpolarizabilities on DFT geometries of NLO-phores with heterocyclic sulfur donors yields somewhat overestimated values.[16] According to TD-DFT calculations, most of the NLO response in TCV-3T and TCV-6T arises from the lowest energy excitation. This excitation causes a one-electron transition from the HOMO, which spreads over the oligothiophene unit to the LUMO, located on the TCV moiety (see Figures 2–4). The lengthening of the oligothiophene chain, going from TCV-3T to TCV-6T, causes a bathochromic shift of the lowest energy absorption and a larger dipole-moment change ($\Delta\mu_{12}$) on excitation, while the transition dipole moment (μ_{12}) remains unchanged. According to the two level approach ($\beta(0) \propto \mu_{12}^2 \ \Delta\mu_{12}/E_{12}^2$), the larger dipole-moment change in TCV-6T is responsible for most of the enhanced hyperpolarizability of this compound.

The large hyperpolarizabilities of symmetrical compounds TCV-3T-TCV and TCV-6T-TCV cannot be explained on the basis of the most stable conformers due to their high symmetry. Compound TCV-6T-TCV is centrosymmetric and hence has zero hyperpolarizability. In a similar way TCV-3T-TCV, while not centrosymmetric, has a very small dipole moment in both the ground and first excited states and, consequently, the lowest energy excitation causes a small dipole-moment change and a low hyperpolarizability (Table 2). To explain the hyperpolarizability of these compounds, we must consider that the high electric fields employed in EFISH experiments stabilize those conformations that have a larger dipole moment.[17] It is therefore possible that the EFISH technique samples molecules in conformations that are not stable in the absence of an electric field.

Through the use of theoretical calculations, we have determined that the conformations with the largest dipole moments are those with a *syn* arrangement of the thiophene rings (displayed here). The *syn* conformers were optimized at the B3LYP/6–31G** level restricted to a nonplanar C_2

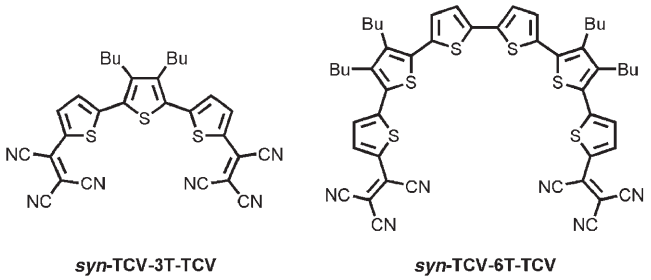

syn-TCV-3T-TCV *syn*-TCV-6T-TCV

symmetry. For TCV-3T-TCV this geometrical arrangement resulted in an increase in the dipole moment from 1.63 to 13.27 Debye, with the energy rising only by 1.63 kcal mol^{-1} with respect to the most stable *anti* conformation. In a similar way, the energy of the *syn* conformation of TCV-6T-TCV was 2.81 kcal mol^{-1} above the most stable *anti* conformation, but the dipole moment increased from 0.0 to 20.15 Debye. The calculated nonlinear optical behavior of these compounds corresponds to that of two-dimensional V-shaped chromophores.[18] The large hyperpolarizabilities calculated for these conformers by using the CPHF method support the experimental values. The lowest-energy electronic absorptions, responsible for the nonlinear optical response, cause the transition of one electron from the HOMO located on the oligothiophene chain to the lowest unoccupied orbitals placed on the tricyanovinyl moieties (Figures 8 and 9).

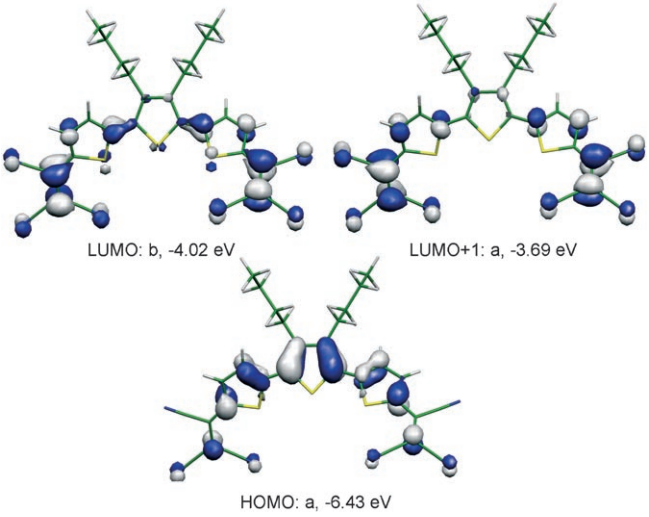

Figure 8. Molecular orbitals of TCV-3T-TCV involved in the nonlinear optical response.

The transition from the HOMO (a symmetry) to the LUMO (b symmetry) calculated at 2.21 eV (TCV-3T-TCV) or 1.73 eV (TCV-6T-TCV), respectively, has B symmetry and therefore contributes to the off-diagonal component of the hyperpolarizability (β_{zyy}). The transition from the HOMO (a) to the LUMO+1 (a) calculated at 2.51 eV (TCV-3T-TCV) or 1.84 eV (TCV-6T-TCV) has A symmetry and contributes to β_{zzz}. It is worth noting that β_{zyy} is much larger than β_{zzz}, mainly due to the larger transition dipole moment associated with the HOMO→LUMO transition compared with HOMO→LUMO+1 transition. Oligothiophenes with a rigid or esterically (i.e., conformationally) constrained *syn* geometry can therefore be proposed as efficient donors in two-dimensional NLO chromophores. Unfortunately, the EFISH experiments described here sample the projection of the hyperpolarizability on the ground-state dipole moment that is approximated as $\beta_z=\beta_{zxx}+\beta_{zyy}+\beta_{zzz}$. We therefore have no conclusive experimental evidence about the two-dimensional character of these chromophores.

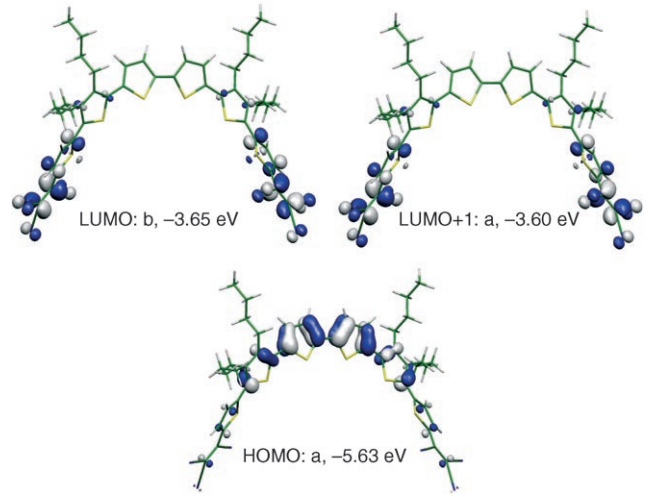

Figure 9. Molecular orbitals of TCV-6T-TCV involved in the nonlinear optical response.

Vibrational properties and molecular structures: The mechanism of charge transfer in these systems can be visualized in terms of extreme canonical forms as a one-electron 3T→TCV transference (Scheme 2), which necessarily proceeds through the generation of a quinoid-like form (zwitterionic state) within the terthienyl path at the expense of the aromatic-like form (apolar state). It is therefore expected that the largest charge flux and IR intensities (permanent dipole-moment changes) to be associated with atomic motions (C=C/C–C stretchings) that mostly mimic this aromatic→quinoid structural evolution. The same aromatic→quinoid interplay concept accounts for the strongest Raman features in polyconjugated molecules, since this coordinate consti-

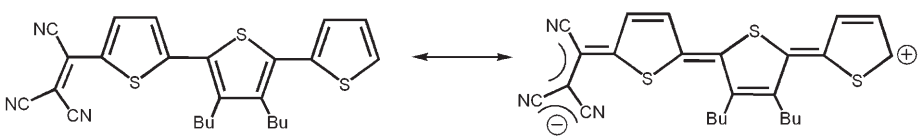

Scheme 2. Resonant forms involved in the ICT process for the prototypical case of TCV-3T

tutes the easiest way to polarize π electrons through the intervention of an electromagnetic field (radiation-induced dipole moments).

The very similar IR and Raman profiles of TCV-3T in Figure 10 is a further confirmation of the occurrence of a very effective intramolecular 3T→TCV charge polarization

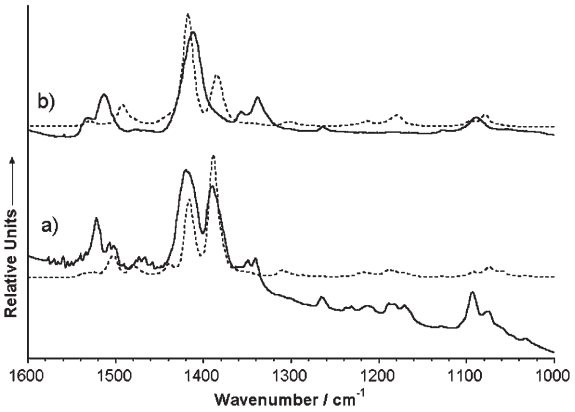

Figure 10. Solid-state vibrational spectra: a) IR (solid line) and Raman (dotted line) spectra of TCV-3T, b) IR (solid line) and Raman (dotted line) spectra of TCV-3T-TCV. λ_{exc} of 1064 nm for the Raman experiments.

in the ground electronic state, in full agreement with its high NLO response. Indeed, the same mechanism of C=C/C−C polarization (already outlined in the previous section) by the presence of two TCV groups is likely to be present in TCV-3T-TCV according to the IR/Raman comparison, although the resemblance is not as noticeable as in the monosubstituted case (i.e., the different molecular symmetry is expected to play a role).

Raman spectra of aromatic oligothiophenes are dominated by a few lines the number of which is almost independent of the number of atoms in the chain. This observation is the result of the existence of a very effective electron–phonon mechanism (coupling between particular C=C/C−C stretch vibrations and the lowest lying electronic excitations).[19] Effective conjugation coordinate (ECC)[20] theory provided a molecular view of this phenomenon according to the following guidelines: 1) A vibrational mode (ECC mode, in-phase symmetric C=C/C−C stretching of the whole conjugated path) exists that mimics the aromatic→quinoid evolution, which is strongly enhanced in the Raman spectrum. 2) The frequency of this mode shifts downward upon increasing conjugated length or increasing quinoidization. This phenomenum is illustrated in Figure 11 by comparing the redox-dependent Raman spectra of α,α′-dimethyl sexithiophene (DMSxT)[19,21,22] with the spectra of the tricyanovinyl-disubstituted oligothiophenes. One-electron oxidation of the full aromatic DMSxT leads to a "*softened*" C−C bond length (aromatic→quinoid transition), while the divalent form strongly inverts the pattern with a clear prevalence of

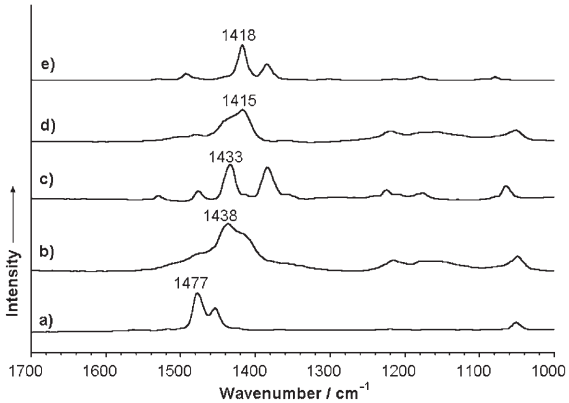

Figure 11. Comparison between the Raman spectra in solid state (λ excitation of 1064 nm) of a) neutral DMSxT, b) $DMSXT^{+\bullet}$, c) TCV-6T-TCV, d) $DMSXT^{+2}$, and e) TCV-3T-TCV.

the quinoid structure spreading over the entire sexithienyl spine.

In agreement with ECC predictions, the strongest bands shift downward from 1477 cm^{-1} in neutral DMSxT to 1438 cm^{-1} in $DMSxT^{\bullet+}$ and to 1415 cm^{-1} in $DMSxT^{2+}$. Accordingly, the ECC mode of TCV-6T-TCV (1433 cm^{-1}) compares best to that of $DMSxT^{\bullet+}$ (1438 cm^{-1}), whereas the collective stretch for TCV-3T-TCV (1418 cm^{-1}) compares best to that of $DMSxT^{2+}$ (1415 cm^{-1}). Therefore, the oligothienyl backbones of the two disubstituted molecules show sizeable quinoidal character depending on the chain length. This structural effect results from the π-mediated tricyanovinyl withdrawal effect (the interacting 3T HOMO and TCV-H LUMO are both of π nature). The π-mediated character of this interaction should be stressed because it can potentially affect the whole oligothiophene spine beyond the rings directly connected to the TCV and in contrast to what should be expected in the case of σ-mediated acceptors. These spectroscopic findings further support the interpretation of the MO frontier orbital interactions upon successive addition of TCV moieties.

Figure 12 compares the Raman spectra of 6T (ECC; 1467 cm^{-1}), TCV-6T (ECC; 1440 cm^{-1}) and TCV-6T-TCV (ECC; 1433 cm^{-1}), and illustrates the frequency downshift upon addition of one and two TCV groups. For the terthienyl series, the ECC mode appears at 1462 cm^{-1} in 3T, 1440 cm^{-1} (weak) in TCV-3T, and 1418 cm^{-1} in TCV-3T-TCV. These spectroscopic data indicate that the most relevant features of the molecular structure are its planarization and quinoidization (Figure 13). These two properties are well supported by theoretical calculations since: 1) Gas-phase-optimized geometries reveal the consecutive planarization upon addition of one and two TCV groups. For example, 3T has calculated dihedral angles between rings of 40°; TCV-3T has dihedral angles of 10° and 40° for the angle closest to and furthest from the TCV group, respectively; and for TCV-3T-TCV the two dihedrals are calculated near 19°. 2) In terms of bond-length-alternation data (BLA, average values between the successive CC conjugated bond

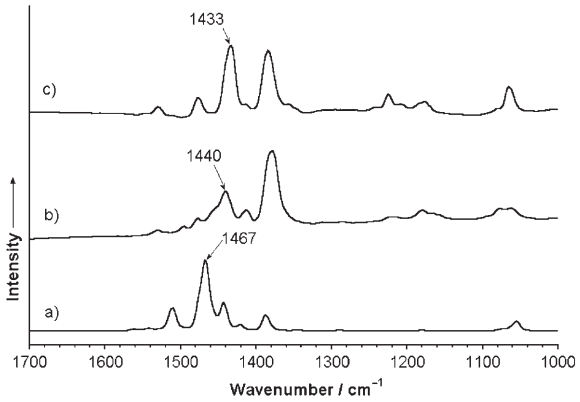

Figure 12. Comparison between the Raman spectra (λ_{exc} of 1064 nm) of a) 6T, b) TCV-6T, and c) TCV-6T-TCV.

lengths, which are positive for aromatic oligomer chains and close to zero upon increasing quinoidization) the BLA decreases in the order 0.0584→0.0405→0.0278 Å for the 3T→TCV-3T→TCV-3T-TCV sequence, in agreement with the spectroscopic findings.

It must be stressed that a splitting of the ECC mode is observed in the asymmetric molecule TCV-3T in accordance with the existence of two "structurally" different thienyl moieties, depending on the proximity to the acceptor (Figure 13). Thus, the BLAs of the thiophenes connected to the TCV in the mono- and disubstituted terthienyls are very similar (0.0035 and 0.0028 Å, respectively), also according to the appearance of the lines at 1416 cm^{-1} and 1418 cm^{-1}, respectively, in the Raman spectra of both systems. As a result, the line at 1440 cm^{-1} in TCV-3T, although weaker, more readily accounts for the quinoid-like structure of the whole terthiophene moiety. Bands around 1390 cm^{-1} arise from $\beta(CH_2)/\beta(CH_3)$ modes of the butyl chains, which are strongly coupled with oligothienyl backbone CC stretching vibrations that describe the ECC dynamic; this coupling might explain their anomalous large intensity.

Apart from the effect of quinoidization, which is the relevant structural effect on TCV↔3T interaction, vibrational spectra provide us with another perspective of the features of the charge polarization in the ground electronic state. This is because the frequency associated with the stretching mode of the cyano groups, ν(CN) around 2200 cm^{-1}, is very sensitive to the total charge borne by the nitriles and transferred by the electron-rich oligothienyl spine.[23,24] The larger the negative charge over the CN group, the lower the wavenumber of its stretching mode. The ν(CN) mode in nonconjugated dicyano methane is recorded at around 2270 cm^{-1}, therefore measurement of this band at 2218 cm^{-1} in TCV-3T and at 2221 cm^{-1} in TCV-3T-TCV is a manifestation of the significant charge transfer towards the three CN groups from the conjugated thienyl path. The 3 cm^{-1} difference between our two chromophores means that the charge transfer does not saturate within the terthienyl chain (i.e., stronger π-withdrawing groups might induce larger ICT), and that the addition of a second TCV group moderately decreases the total amount of charge on the CN groups with respect to the monosubstituted system. This finding is supported by the theoretical Mülliken atomic charges over the TCV moiety, which for TCV-3T is −0.264 e (−0.177, −0.176, and −0.210 e for each CN group) and for TCV-3T-TCV is −0.220 e (−0.166, −0.162, and −0.202 e for each CN group). From this line of reasoning, even smaller differences regarding the ν(CN) bands in the sexithienyl parents are expected (2216 and 2215 cm^{-1} in TCV-6T and TCV-6T-TCV).

This spectroscopic description is consistent with the quantitative red shifts of the charge transfer band in our samples (namely, 571→583 nm with the 3 cm^{-1} in TCV-3T→TCV-3T-TCV and 624→628 nm with the 1 cm^{-1} in TCV-6T→TCV-6T-TCV) and is useful for the analysis of the acceptor actuation. To evaluate the effect of the ICT on the donor moiety, the ECC frequency downshift analysis predicts a

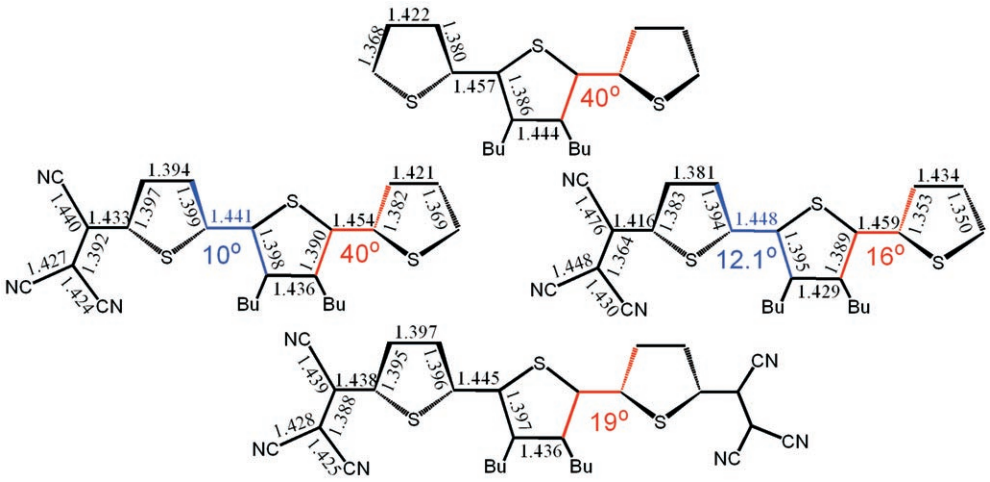

Figure 13. B3LYP/6–31G** optimized geometries for the three investigated trimers. Relevant dihedral angles are shown. For TCV-3T, the right-hand scheme corresponds to experimental data.

moderate quinoidization of the terthienyl backbone upon monosubstitution. Furthermore, quinoidization becomes more pronounced in the doubly substituted compound. This is not in support of an increased overall ICT, however, since the electron-donation capacity of the thienyl chain is now shared by the two competing electron acceptors.

Conclusions

This investigation compares the molecular and electronic properties of mono- and disubstituted tricyanovinyl (TCV) oligomers with three or six thiophene rings. Specifically, we have addressed how these properties and intramolecular π-donor and π-acceptor interactions are tuned as a function of the symmetric and asymmetric patterns. These key features, which have direct consequences on their performance in electrooptical applications, are addressed by the analysis of the their spectroscopic (UV/Vis absorption, IR and Raman), electrochemical, solid state and nonlinear optical properties. An understanding of the electronic and molecular properties is supported with the help of quantum chemistry (DFT theory).

The tricyanovinyl→oligothiophene interaction is mediated by the electronic coupling of the empty LUMOs of TCV-H and the HOMO of 3T. The bonding interaction between both terms enables us to explain the large red shift of the HOMO–LUMO lowest energy band upon addition of one TCV unit, which remains nearly unaffected upon disubstitution. The electrochemical and vibrational properties are also consistent with this MO description. The TCV samples display amphoteric redox behavior with a noticeable low electrochemical gap for the monosubstituted system with six thiophenes. It turns out that the best scenario for simultaneous injection/extraction of electrons is found for TCV-6T (based on electrochemical data). This property, combined with its strong low-energy optical absorption, represents a promising feature highly desirable in, for example, photon-to-charge conversion devices (solar cells). Unexpectedly, nonlinear optical results reveal the symmetric samples to be active and have been rationalized on the basis of the conformational flexibility of these compounds. The symmetric samples, however, display high NLO response due to the intramolecular charge transfer character of the $S_0 \rightarrow S_1$ excitation.

The analysis of the vibrational data reflects the interplay between the aromatic and quinoid canonical forms in the description of their electronic structure. This is a common feature in the chemistry of polyconjugated heterocycles. Interesting here, however, is that both canonical forms are suitably balanced, interchanging their weights according to the TCV functionalization and chain dimension. The understanding of these key issues, in particular electronic structure, is fundamentally important in the design and implementation of new organic materials. To the general reader, this paper combines physical methods with modern theoretical approaches to better understand advanced molecules and materials, which will play a prominent role in the future technological scenario.

Experimental Section

Synthesis: Synthetic procedures were carried out under an inert atmosphere of nitrogen. Tetrahydrofuran was distilled from Na/benzophenone and anhydrous dichloromethane was purchased from Acros and used as received. Oligomers 3T[13a] and 6T[14] were prepared as previously described. Tetracyanoethylene and *n*-butyllithium (2.5 M in hexanes) were purchased from Aldrich and used as received. NMR spectra were recorded on a JEOL Eclipse 300 MHz instrument. The chemical shifts are reported in ppm and referenced to the residual chloroform peak ($\delta =$ 7.26 ppm). Mass spectra were obtained on a Finnigan MAT 95 mass spectrometer. Elemental analyses were performed by Quantitative Technologies, Inc., Whitehouse, NJ.

TCV-3T: *n*-Butyllithium (0.58 mL, 1.5 mmol) was added over 30 min to a dry two-necked round-bottom flask containing 3T (0.528 g, 1.46 mmol) and THF (10 mL) at −78 °C. The reaction mixture was warmed to 0 °C and was stirred for 0.5 h. The suspension was then cooled back to −78 °C, and tetracyanoethylene (0.224 g, 1.75 mmol) was added in one portion, resulting in an immediate color change from yellow to dark green. Dichloromethane (8 mL) was added to the reaction after 30 min, and the mixture was neutralized with 0.05 M HCl. The solvents were then removed by rotary evaporation. The crude solid was then dissolved in dichloromethane, and the mixture was dried with $MgSO_4$ and concentrated. The crude solid was purified by column chromatography (silica gel, toluene) to afford 0.350 g (51.8 %) of TCV-3T as a dark olive-green solid. ^{1}H NMR (300 MHz, $CDCl_3$): $\delta = 8.00$ (d, $J = 4.4$ Hz, 1H), 7.42 (dd, $J =$ 1.1, 5.2 Hz, 1H), 7.36 (d, $J = 4.4$ Hz, 1H), 7.24 (dd, $J = 1.1$, 3.7 Hz, 1H), 7.11 (dd, $J = 3.8$, 5.1 Hz, 1H), 2.84 (t, $J = 7.8$ Hz, 2H), 2.74 (t, $J = 8.0$ Hz, 2H), 1.48 (m, 8H), 0.97 ppm (m, 6H); HREIMS: *m*/*z* calcd: 461.1054; found: 461.1089 $[M]^+$; elemental analysis calcd (%) for $C_{25}H_{23}N_3S_3$: C 65.04, H 5.02, N 9.10; found: C 65.40, H 5.01, N 8.98.

TCV-6T: The oligomer was prepared from 6T (0.300 g, 0.417 mmol), *n*-butyllithium (0.17 mL, 0.43 mmol), and tetracyanoethylene (0.065 g, 0.51 mmol) by using the general procedure as described above for the synthesis of TCV-3T. The crude solid was purified by column chromatography (silica gel, toluene) to afford 79 mg (23 %) of TCV-6T as a dark purple solid. ^{1}H NMR (300 MHz, $CDCl_3$): $\delta = 8.05$ (d, $J = 4.7$ Hz, 1H), 7.36 (d, 4.7 Hz, 1H), 7.32 (dd, $J = 1.1$, 5.2 Hz, 1H), 7.16 (m, 4H), 7.07 (m, 2H), 2.77 (m, 8H), 1.51 (m, 16H), 0.99 ppm (m, 12H); HREIMS: *m*/*z* calcd: 819.1938; found: 819.1898 $[M]^+$; elemental analysis calcd (%) for $C_{45}H_{45}N_3S_6$: C 65.89, H 5.53, N 5.12; found: C 65.87, H 5.10, N, 4.83.

Spectroscopic measurements: UV/Vis absorption measurements were recorded on an Ocean Optics USB2000 fiber optic spectrometer. FT-IR spectra were performed using an ATR cell incorporated in a Bruker Equinox 55 FT-IR interferometer, and the FT-Raman spectra were measured using an FT-Raman accessory kit (FRA/106-S) of the same apparatus. A continuous-wave Nd-YAG laser working at 1064 nm was employed for excitation. A germanium detector operating at liquid nitrogen temperature was used. Raman scattering radiation was collected in a backscattering configuration with a standard spectral resolution of 4 cm^{-1}. In order to avoid possible damage to the samples upon laser radiation, laser power was kept to a level lower than 100 mW and 1000–3000 scans were averaged for each spectrum.

X-ray crystallographic data collection and refinement: Crystal data and other details of the structure analysis are summarized in Table 3. A red-purple single crystal of TCV-3T (0.085 mm × 0.060 mm × 0.025 mm) was placed onto the tip of a 0.1 mm diameter glass capillary and mounted on a Siemens SMART Platform CCD diffractometer for a data collection at 173(2) K. A preliminary set of cell constants was calculated from reflections harvested from three sets of 20 frames. These initial sets of frames were oriented such that orthogonal wedges of reciprocal space were surveyed. This produced initial orientation matrices determined from 30 reflections. The data collection was carried out by using $Mo_{K\alpha}$ radiation

Table 3. Crystal data and structure refinement for TCV-3T.

formula	$C_{25}H_{23}N_3S_3$	Z	8
M_r	461.64	ρ_{calcd} [g cm^{-3}]	1.309
crystal system	monoclinic	$2\theta_{max}$	50.08
space group	$C2/c$	reflns collected	11343
a [Å]	23.068(3)	unique reflns	4125
b [Å]	7.7555(9)	obsvd reflns [$I>2\sigma(I)$]	2224
c [Å]	26.225(3)	parameters/restraints	294/10
α [°]	90	μ(Kα) [cm^{-1}]	3.34
β [°]	93.272(2)	$R1$[a]/GoF[b]	0.0582/0.954
γ [°]	90	$wR2$[c] [$I>2\sigma(I)$]	0.1651
V [Å^3]	4684.1(10)	residual density [e Å^{-3}]	+0.472/−0.371

[a] Observation criterion: $I>2\sigma(I)$. $R1=\Sigma||F_o|-|F_c||/\Sigma|F_o|$. [b] Goodness of fit (GoF) $=[\Sigma[w(F_o^2-F_c^2)^2]/(n-p)]^{1/2}$. [c] w$R2=[\Sigma[w(F_o^2-F_c^2)^2]/\Sigma[w(F_o^2)^2]]^{1/2}$ in which $w=q/[\sigma^2(F_o2)+(aP)^2+bP+d+e\sin(\theta)]$.

($\lambda=0.71073$ Å) with a graphite monochromator, a frame time of 60 s, and a detector distance of 4.893 cm. A randomly oriented region of reciprocal space was surveyed to the extent of one sphere and to a resolution of 0.84 Å. Four major sections of frames were collected with 0.30° steps in ω at four different ϕ settings and a detector position of −28° in 2θ. The intensity data were corrected for absorption and decay using the program SADABS. The minimum and maximum transmission values obtained from the absorption correction were 0.7638 and 1.0000. Final cell constants were calculated from the xyz centroids of 2816 strong reflections from the actual data collection after integration using the program SAINT. The structure was solved using SHELXS-97 and refined using SHELXL-97. The space group $C2/c$ was determined based on systematic absences and intensity statistics. A direct-methods solution was calculated which provided most non-hydrogen atoms from the E-map. Full-matrix least-squares/difference Fourier cycles were performed which located the remaining non-hydrogen atoms. All non-hydrogen atoms were refined with anisotropic displacement parameters. All hydrogen atoms were placed in ideal positions and refined as riding atoms with relative isotropic displacement parameters. The final full matrix least squares refinement converged to $R1=0.0582$ and $wR2=0.1651$ (F^2, all data). CCDC-276900 contains the supplementary crystallographic data for this paper. These data can be obtained free of charge from The Cambridge Crystallographic Data Centre via www.ccdc.cam.ac.uk/data_request/cif.

Cyclic voltammetry measurements: Room-temperature electrochemical measurements were performed with a BAS 100B electrochemical analyzer using methods previously described.[25] Potentials are reported versus aqueous Ag/AgCl and are not corrected for the junction potential. The $E^{\circ\prime}$ value for the ferrocenium/ferrocene couple for concentrations similar to those used in this study was 0.46 V for dichloromethane solutions at a glassy carbon electrode.

EFISH measurements: Measurements were performed with a nonlinear optics spectrometer from SOPRA. The fundamental light at 1.907 μm was the first Stokes peak of a hydrogen Raman cell pumped by the 1.064 μm light from a Q-switched Nd:YAG laser (Quantel YG 781, 10 pps, 8 ns, pulse). That light was passed through a linear polarizer and focused on the EFISH cell. The polarizing dc voltage (parallel to the light polarization) used in this cell was 6 kV. The output light from the cell was passed through an interference filter to select the second harmonic light (0.954 μm), which was finally detected with a R642 photomultiplier from Hamamatsu. Static $\mu\beta(0)$ values were deduced from the experimental values using a two-level dispersion model.

Theoretical methodology: Density functional theory (DFT) calculations were carried out by means of the Gaussian 98 program[26] running on a SGI Origin 2000 supercomputer. We used the Becke's three-parameter exchange functional combined with the LYP correlation functional (B3LYP).[27] It has already been shown that the B3LYP functional yields similar geometries for medium-sized molecules as MP2 calculations do with the same basis sets.[28,29] We also made use of the standard 6–31G** basis set.[30] Optimal geometries were determined on isolated entities in the vacuum. All geometrical parameters were allowed to vary independently apart from planarity of the rings, unless otherwise stated. Vertical electronic excitation energies were computed by using the time-dependent DFT (TDDFT) approach[31–33] and excited-state dipole moments were calculated using the RHOCI density. Molecular hyperpolarizabilities were calculated by using the CPHF analytical derivative method.

Acknowledgements

J.C. is grateful to the Ministerio de Ciencia y Tecnología (MCyT) of Spain for a Ramón y Cajal research position of Chemistry at the University of Málaga. The present work was supported in part by the Dirección General de Enseñanza Superior (DGES, MEC, Spain) through the research projects BQU2003–03194 and BQU2002-00219. We are also indebted to Junta de Andalucía (Spain) (FQM-0159) and Gobierno de Aragón (E39) funding for our research groups. M.C.R.D. thanks the MEC of Spain for a personal grant. T.M.P. acknowledges a Grant-in-Aid of Research, Artistry and Scholarship from the Office of the Dean of the Graduate School of the University of Minnesota.

[1] K. Mullen, G. Wegner, *Electronic Materials: The Oligomer Approach*, Wiley-VCH, Weinheim, **1998**; D. Fichou, *Handbook of Oligo- and Polythiophenes*, Wiley-VCH, Weinheim, **1999**; H. S. Nalwa, *Handbook of Advanced Electronic and Photonic Materials and Devices*, Academic, San Diego, **2000**.

[2] See for example: a) J. Roncali, *Chem. Rev.* **1997**, *97*, 173; b) C. D. Dimitrakopoulos, P. R. L. Malefant, *Adv. Mater.* **2002**, *14*, 99; c) M. Mushrush, A. Facchetti, M. Lefenfeld, H. E. Katz, T. J. Marks, *J. Am. Chem. Soc.* **2003**, *125*, 9414; d) A. Yassar, F. Demanze, A. Jaafari, M. El Idrissi, C. Coupry, *Adv. Funct. Mater.* **2002**, *12*, 699.

[3] a) F. Garnier, G. Horowitz, X. Z. Peng, D. Fichou, *Adv. Mater.* **1990**, *2*, 592; b) F. Garnier, *Acc. Chem. Res.* **1999**, *32*, 209, and references therein; c) F. Garnier, R. Hajlaoui, A. Yassar, P. Srivastava, *Science* **1994**, *265*, 684; d) A. Dodabalapur, L. Torsi, H. E. Katz, *Science* **1995**, *268*, 270; e) H. E. Katz, Z. Bao, S. L. Gilat, *Acc. Chem. Res.* **2001**, *34*, 359; f) A. Facchetti, M. Mushrush, H. E. Katz, T. J. Marks, *Adv. Mater.* **2003**, *15*, 33; g) A. Facchetti, Y. Deng, A. Wang, Y. Koide, H. Sirringhaus, T. J. Marks, R. H. Friend, *Angew. Chem.* **2000**, *112*, 4721; *Angew. Chem. Int. Ed.* **2000**, *39*, 4547; h) C. R. Newman, C. D. Frisbie, D. A. da Silva Filho, J. L. Brédas, P. C. Ewbank, K. R. Mann, *Chem. Mater.* **2004**, *16*, 4436.

[4] a) J. H. Burroughes, D. D. C. Bradley, A. R. Brown, R. N. Marks, K. Mackay, R. H. Friend, P. L. Burns, R. B. Holmes, *Nature* **1990**, *347*, 539; b) N. S. Sariciftci, L. Smilowitz, A. J. Heeger, F. Wudl, *Science* **1992**, *258*, 1474; c) A. P. Kulkarni, C. J. Tonzola, A. Babel, S. A. Jenekhe, *Chem. Mater.* **2004**, *16*, 4556; d) J. M. Tour, *Acc. Chem. Res.* **2000**, *33*, 791; e) D. Pisignano, M. Anni, G. Gigli, R. Cingolani, M. Zavelani-Rossi, G. Lanzani, G. Barbarella, L. Favaretto, *Appl. Phys. Lett.* **2002**, *81*, 3534; f) M. Pasini, S. Destri, W. Porzio, C. Botta, U. Giovanella, *J. Mater. Chem.* **2003**, *13*, 807; g) M. Suzuki, M. Fukuyama, Y. Hori, S. Hotta, *J. Appl. Phys.* **2002**, *91*, 5706; h) K. Hara, M. Kurashige, Y. Dan-Oh, C. Kasada, A. Shinpo, S. Suga, K. Sayama, H. Arakawa, *New J. Chem.* **2003**, *27*, 783.

[5] a) S. R. Marder, J. E. Sohn, G. D. Stucky, *Materials for Nonlinear Optics-Chemical Perspectives*, American Chemical Society, Washington, **1991**; b) S. R. Marder, W. E. Torruellas, M. Blanchard-Desce, V. Ricci, G. I. Stegeman, S. Gilmour, J. L. Brédas, J. Li, G. U. Bublitz, S. G. Boxer, *Science* **1997**, *276*, 1233.

[6] See for instance: a) F. Effenberger, F. Wurthner, F. Steybe, *J. Org. Chem.* **1995**, *60*, 2082; b) J. Casado, T. M. Pappenfus, L. L. Miller, K. R. Mann, E. Ortí, P. M. Viruela, R. P. Amérigo, V. Hernández, J. T. López Navarrete, *J. Am. Chem. Soc.* **2003**, *125*, 2524.

[7] a) M. Albolta, D. Beljonne, J. L. Brédas, J. E. Ehrlich, J. Y. Fu, A. A. Heikal, S. E. Hess, T. Kogej, M. D. Levin, S. R. Marder, J. W. Perry, H. Rockel, M. Rumi, G. Subramaniam, W. W. Webb, X. L. Wu, C. Xu, *Science* **1998**, *281*, 1653; b) A. Abbotto, L. Beverina, R. Bozio,

A. Fachetti, C. Ferrante, G. A. Pagani, D. Pedron, R. Signorini, *Chem. Commun.* **2003**, *13*, 825; c) M. Rumi, J. E. Ehrlich, A. A. Heikal, J. W. Perry, S. Barlow, Z. Hu, D. McCord-Maughon, T. C. Parker, H. Rockel, S. Thayumanavan, S. R. Marder, D. Beljonne, J. L. Brédas, *J. Am. Chem. Soc.* **2000**, *122*, 9500.
[8] W. Denk, J. H. Strickler, W. W. Webb, *Science* **1990**, *248*, 73.
[9] J. E. Ehrlich, *Opt. Lett.* **1997**, *22*, 1843.
[10] D. A. Parthenopoulos, P. M. Rentzepis, *Science* **1989**, *245*, 843.
[11] a) R. J. Chesterfield, C. R. Newman, T. M. Pappenfus, P. C. Ewbank, M. H. Haukaas, K. R. Mann, L. L. Miller, C. D. Frisbie, *Adv. Mater.* **2003**, *15*, 1278; b) T. M. Pappenfus, R. J. Chesterfield, C. D. Frisbie, K. R. Mann, J. Casado, J. D. Raff, L. L. Miller, *J. Am. Chem. Soc.* **2002**, *124*, 4184.
[12] a) H. E. Katz, K. D. Singer, J. E. Sohn, C. D. Dirk, L. A. King, H. M. Gordon, *J. Am. Chem. Soc.* **1987**, *109*, 6561; b) S. R. Marder, C. B. Gorman, B. G. Tiemann, L.-T. Cheng, *J. Am. Chem. Soc.* **1993**, *115*, 3006; c) V. P. Rao, A. K-Y. Jen, K. Y. Wong, K. J. Drost, *J. Chem. Soc. Chem. Commun.* **1993**, 1118; d) C. Cai, I. Liakatas, M.-S. Wong, M. Bosch, C. Bosshard, P. Gunter, S. Concilio, N. Tirelli, U. W. Suter, *Org. Lett.* **1999**, *1*, 1847; e) K. Eckert, A. Schroder, H. Hartmann, *Eur. J. Org. Chem.* **2000**, 1327; f) J. Ohshita, K.-H. Lee, M. Hashimoto, Y. Kunugi, Y. Harima, K. Yamashita, A. Kunai, *Org. Lett.* **2002**, *4*, 1891.
[13] a) T. M. Pappenfus, M. W. Burand, D. E. Janzen, K. R. Mann, *Org. Lett.* **2003**, *5*, 1535; b) M. M. Bader, R. Custelcean, M. D. Ward, *Chem. Mater.* **2003**, *15*, 616; c) X. Cai, M. W. Burand, T. M. Pappenfus, C. R. Newman, M. M. Bader, K. R. Mann, C. D. Frisbie, *J. Phys. Chem. B*, in press.
[14] T. M. Pappenfus, K. R. Mann, *Inorg. Chem.* **2001**, *40*, 6301.
[15] T. Koopmans, *Physica* **1933**, *1*, 104.
[16] M. González, J. L. Segura, C. Seoane, N. Martín, J. Garín, J. Orduna, R. Alcalá, B. Villacampa, V. Hernández, J. T. López Navarrete, *J. Org. Chem.* **2001**, *66*, 8872.
[17] J. O. Morley, M. G. Hutchings, J. Zyss, I. Ledoux, *J. Chem. Soc. Perkin Trans. 2* **1997**, 1139.
[18] a) B. J. Coe, J. A. Harris, B. S. Brunschwig, J. Garín, J. Orduna, *J. Am. Chem. Soc.* **2005**, *127*, 3284; b) B. J. Coe, J. A. Harris, L. A. Jones, B. S. Brunschwig, K. Song, K. Clays, J. Garín, J. Orduna, S. J. Coles, M. B. Hursthouse, *J. Am. Chem. Soc.* **2005**, *127*, 4845.
[19] a) V. Hernández, J. Casado, F. J. Ramírez, G. Zotti, S. Hotta, J. T. López Navarrete, *J. Chem. Phys.* **1996**, *104*, 9271; b) C. Moreno Castro, M. C. Ruiz Delgado, V. Hernández, S. Hotta, J. Casado, J. T. López Navarrete, *J. Chem. Phys.* **2002**, *116*, 10419; J. Casado, H. E. Katz, V. Hernández, J. T. López Navarrete, *J. Phys. Chem. B* **2002**, *106*, 2488.
[20] C. Castiglioni, M. Gussoni, J. T. López Navarrete, G. Zerbi, *Solid State Commun.* **1988**, *65*, 625.
[21] J. Casado, V. Hernandez, S. Hotta, J. T. López Navarrete, *J. Chem. Phys.* **1998**, *109*, 10419.
[22] J. Casado, V. Hernández, S. Hotta, J. T. López Navarrete, *Adv. Mater.* **1998**, *10*, 1258.
[23] a) T. Takenaka, *Spectrochim. Acta Part A* **1971**, *27*, 1735; b) A. Girlando, C. Pecile, *Spectrochim. Acta Part A* **1973**, *29*, 1859.
[24] J. Casado, L. L. Miller, K. R. Mann, T. M. Pappenfus, H. Higuchi, E. Ortí, B. Milián, R. Pou-Amérigo, V. Hernández, J. T. López Navarrete, *J. Am. Chem. Soc.* **2002**, *124*, 12380.
[25] D. D. Graf, R. G. Duan, J. P. Campbell, L. L. Miller, K. R. Mann, *J. Am. Chem. Soc.* **1997**, *119*, 5888.
[26] Gaussian 98, Revision A.7, M. J. Frisch, G. W. Trucks, H. B. Schlegel, G. E. Scuseria, M. A. Robb, J. R. Cheeseman, V. G. Zakrzewski, J. A. Montgomery, R. E. Stratman, S. Burant, J. M. Dapprich, J. M. Millam, A. D. Daniels, K. N. Kudin, M. C. Strain, O. Farkas, J. Tomasi, V. Barone, M. Cossi, R. Cammi, B. Mennucci, C. Pomelli, C. Adamo, S. Clifford, G. Ochterski, A. Petersson, P. Y. Ayala, Q. Cui, K. Morokuma, D. K. Malick, A. D. Rabuck, K. Raghavachari, J. B. Foresman, J. Cioslowski, J. V. Ortiz, B. B. Stefanov, G. Liu, A. Liashenko, I. Piskorz, I. Komaromi, R. Gomperts, R. L. Martin, D. J. Fox, T. Keith, M. A. Al-Laham, C. Y. Peng, A. Manayakkara, C. González, M. Challacombe, P. M. W. Gill, B. G. Johnson, W. Chen, M. W. Wong, J. L. Andres, M. Head-Gordon, E. S. Replogle, J. A. Pople, Gaussian Inc., Pittsburgh, **1998**.
[27] A. D. Becke, *J. Chem. Phys.* **1993**, *98*, 1372.
[28] P. J. Stephens, F. J. Devlin, F. C. F, Chabalowski, M. J. Frisch, *J. Phys. Chem.* **1994**, *98*, 11623.
[29] J. J. Novoa, C. Sosa, *J. Phys. Chem.* **1995**, *99*, 15837.
[30] M. M. Francl, W. J. Pietro, W. J. Hehre, J. S. Binkley, M. S. Gordon, D. J. Defrees, J. A. Pople, *J. Chem. Phys.* **1982**, *77*, 3654.
[31] a) E. Runge, E. K. U. Gross, *Phys. Rev. Lett.* **1984**, *52*, 997; b) E. K. U. Gross, W. Kohn, *Adv. Quantum Chem.* **1990**, *21*, 255; c) *Density Functional Theory* (Eds.:E. K. U. Gross, R. M. Driezler), Plenum, New York, **1995**.
[32] M. E. Casida, *Recent Advances in Density Functional Methods*, *Part I*, World Scientific, Singapore, **1995**.
[33] W. Koch, M. C. Holthausen, *A Chemist's Guide to Density Functional Theory*, Wiley-VCH, Weinheim, **2000**.

Received: November 8, 2005
Published online: April 21, 2006

